Electronic Supplementary Material (ESI) for ChemComm.

Isomorphous Template Induced Crystallisation: A Robust Method for the Targeted Crystallisation of Computationally Predicted Metastable Polymorphs

*Vijay K. Srirambhatla,[a] Rui Guo,[b] Sarah L. Price[b] and Alastair J. Florence[a]**

[a]Solid-State Research Group, Strathclyde Institute of Pharmacy and Biomedical Sciences, University of Strathclyde, 99 George Street, Glasgow, G1 1RD, UK.

[b]Department of Chemistry, University College London, 20 Gordon St, London, WC1H 0AJ, UK.

Contents

I. Experimental:

1. Polycrystalline template preparation and characterisation:

   Around 120 mg of dihydrocarbamazepine was ground in presence of 1 ml of ethylacetate solution using a mortar and pestle for about 2 minutes until a thick slurry of DHC was obtained.

   Using a glass capillary, the DHC slurry of ethylacetate was drop casted or smear coated on a glass slide to obtain a layer of DHC. Powder X-ray analysis (Figure S1) of the drop casted DHC thin layer confirms that the polymorphic form as DHC-II. SEM analysis (Figure S2) of the thin layer indicates the presence of facets and suggests that the surface is highly heterogeneous.

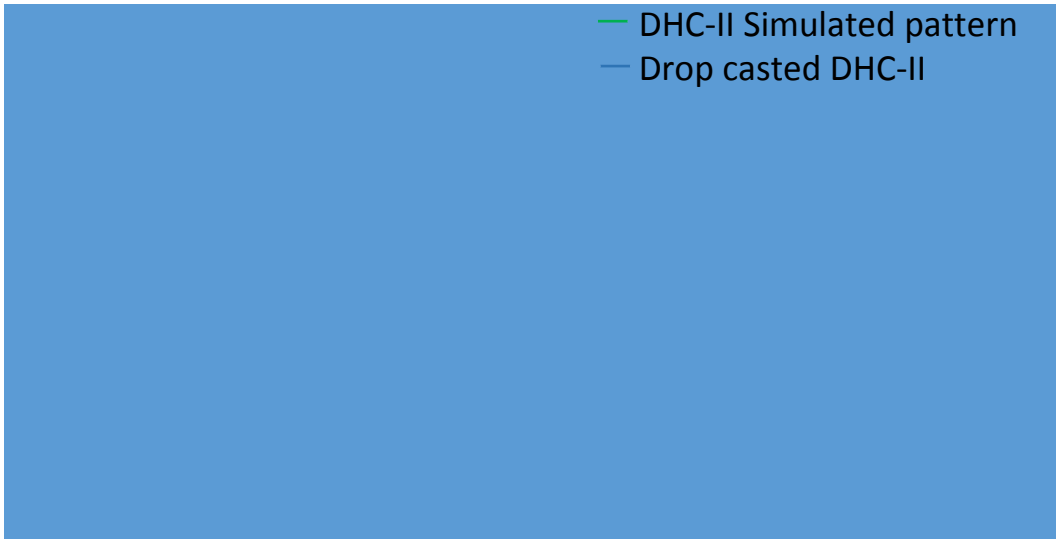

Figure S1: PXRD comparison plot

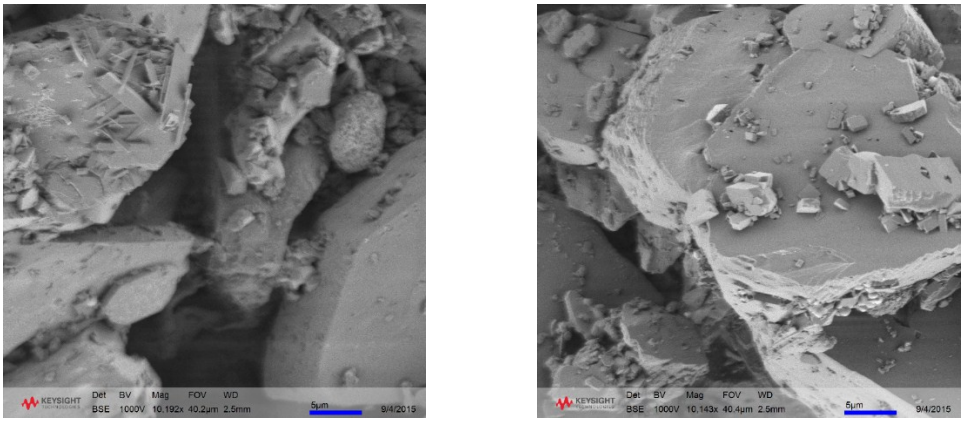

Figure S2: SEM of DHC-II polycrystalline template.

2. Sublimation experimental set-up and results:

   Around 40-50mg of CBZ-V was placed on the petri dish whilst holding the temperature of the heating plate at 125 ^{o}C, with the polycrystalline template sitting on the petri dish as shown in figure S3. After 48 hrs of vapour deposition of CBZ on DHC-II template, the top layer of the deposited crystals (Figure S4) were analysed by capillary powder X-ray diffraction (Figure S5), which indicated the presence of CBZ-V and CBZ-I.

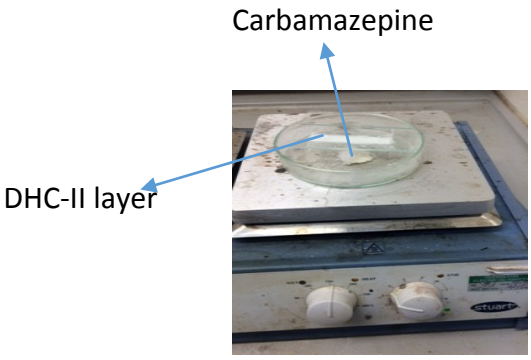

Figure S3: Sublimation experimental set-up.

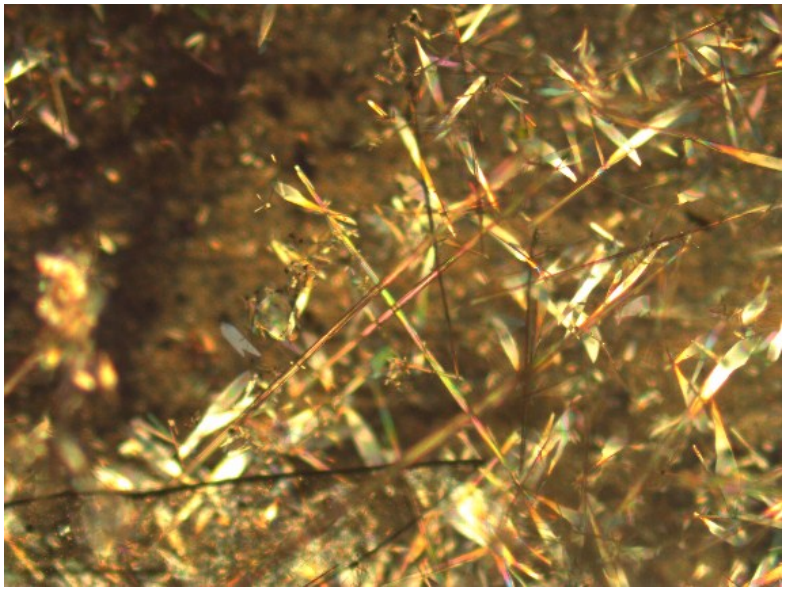

Figure S4: Deposited CBZ crystals on polycrystalline DHC-II template.

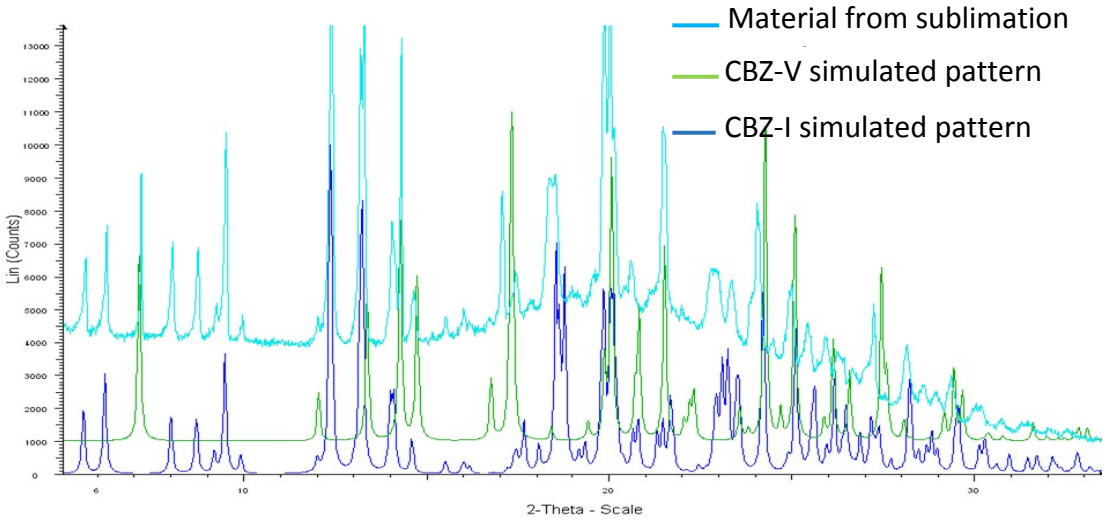

Figure S5: PXRD comparison plot.

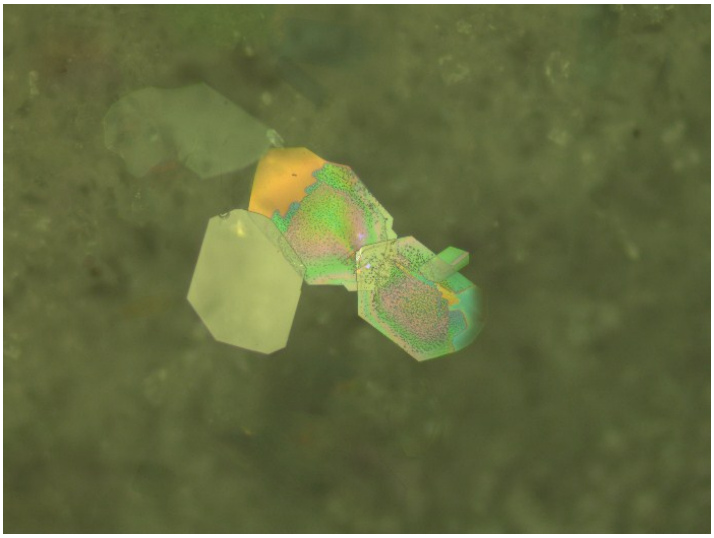

Figure S6: Deposited CYH crystals on polycrystalline DHC-II template.

Several vapour deposition experiments were performed using the above experimental setup during the method development whilst altering the temperature and vapour deposition time. The temperature of the heating plate was varied between 120-145 ^{o}C whilst the vapour deposition time was varied between 30-48 hrs. The optimal conditions for the formation of form V are reported here and in the manuscript. The presence of CBZ I and V was observed in the deposited material throughout testing of the polycrystalline DHC II template. The polycrystalline material maximises the possibility for surface templating and in effect acts as a screen to maximise the possibility of templating effect. However, in order to understand the templating effect a more ordered array of DHC-II crystals grown on the glass slide were used as a template.

3. Template with crystals grown on glass slide.

a) Template preparation:

A clear solution of DHC in ethylacetate was obtained by dissolving around 100 mg of DHC-II in 6 ml of ethyl acetate whilst warming up the solution at around 40 ^{o}C. A glass slide was then immersed at the bottom of the beaker and the solution was allowed to crystallise by slow evaporation method whilst standing at room temperature. The DHC-II crystals grown on the glass slide (figure S7) were analysed by powder X-ray diffraction (figure S8).

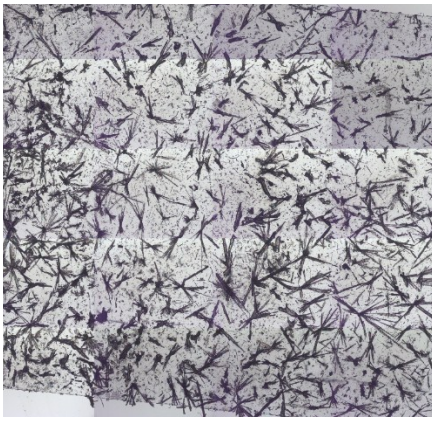

Figure S7: Template with multiple DHC-II single crystals on glass slide.

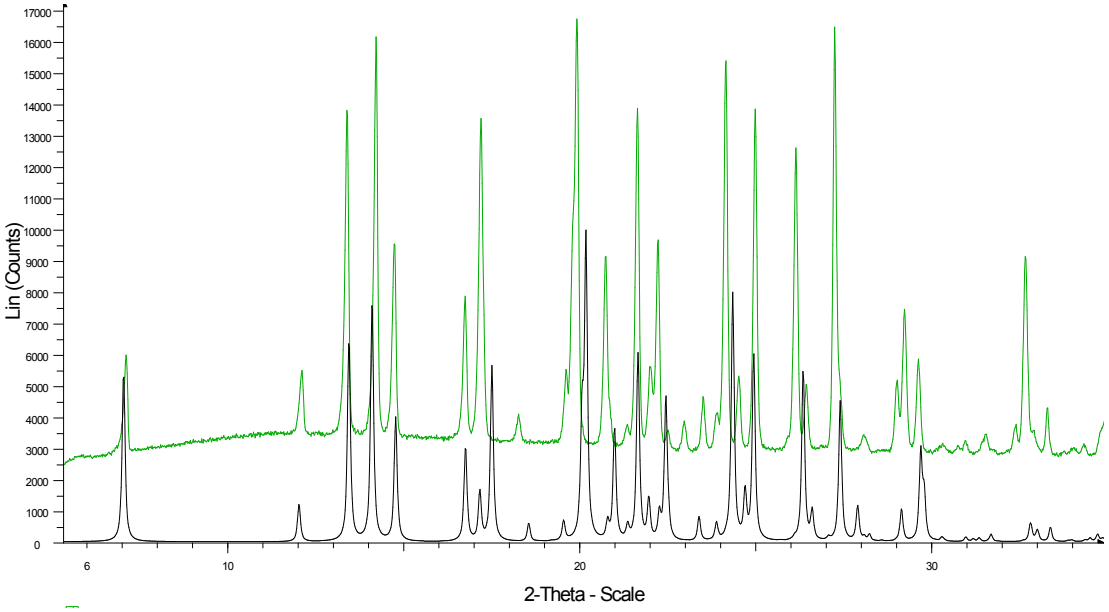

Figure S8: PXRD comparison plot of DHC-II single crystals from ethyl acetate (green) with single crystal simulated powder pattern (black).

b) Face indexing of crystals from ethylacetate:
Representative single crystals grown form ethyl acetate solution, suitable for face indexing were face indexed using the Bruker Apex 3 software suite.

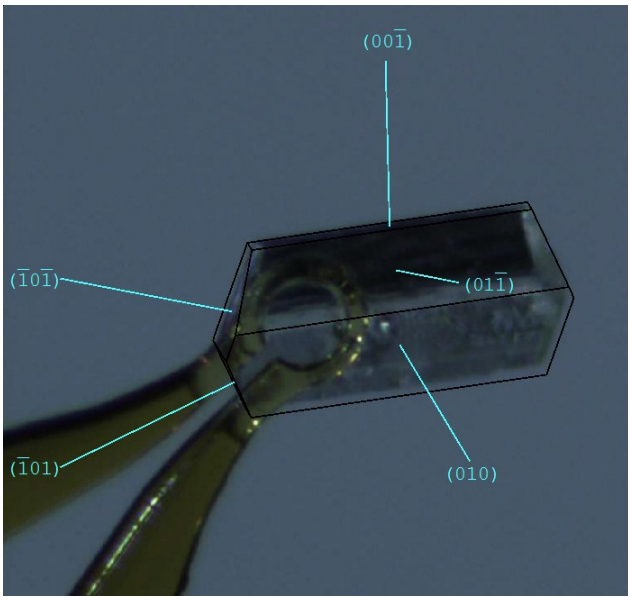

(a)

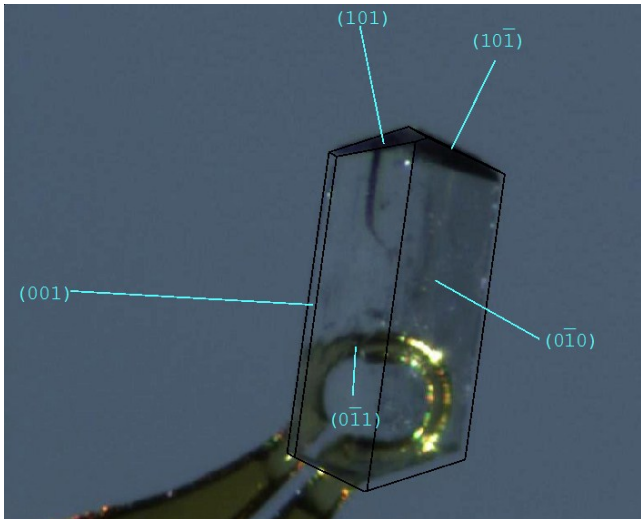
(1$\bar{0}$1)
(10$\bar{1}$)
(001)
(0$\bar{1}$0)
(0$\bar{1}$1)

(b)

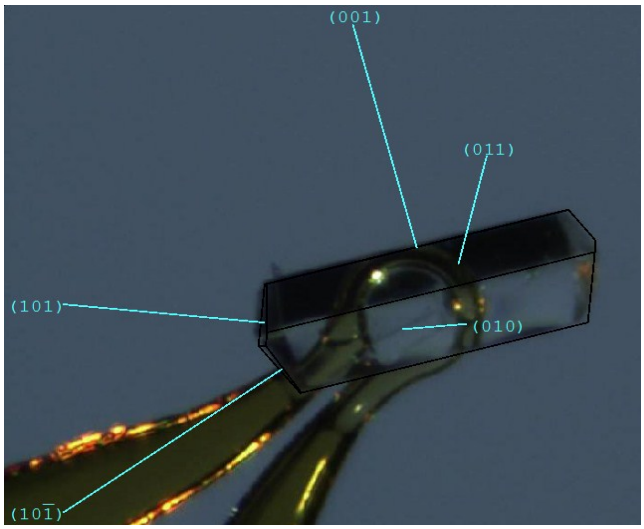
(001)
(011)
(101)
(010)
(10$\bar{1}$)

(c)

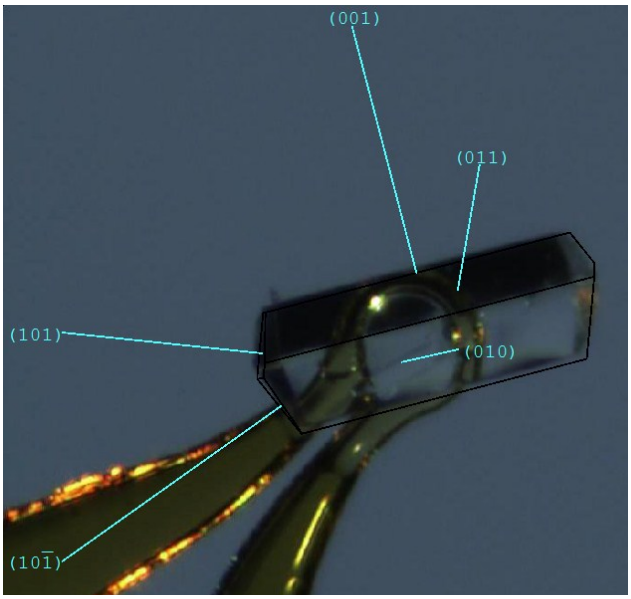
(001)
(011)
(101)
(010)
(10$\bar{1}$)

(d)

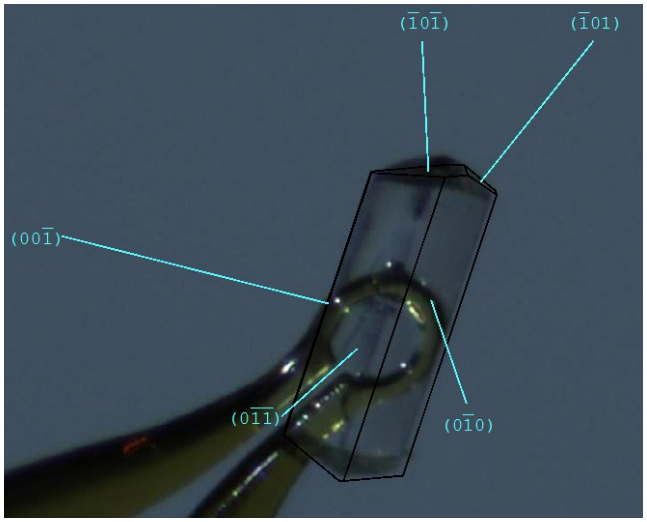

(e)

Figure S9 (a) – (e): face indexing of DHC-II single crystals from ethylacetate.

c) AFM analysis of DHC-II single crystals from ethylacetate solution.
The AFM images (Figure S10) on some of the DHC-II single crystals showed ledges on the (010) and (011) faces with varying ledge heights (20nm – 96nm) and angles (110 – 130°).

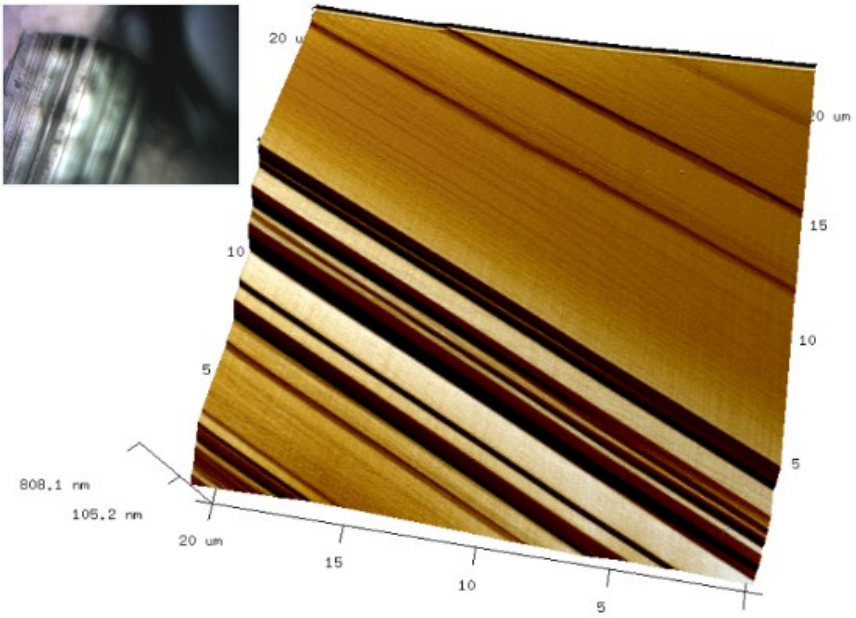

Figure S10: AFM image of DHC-II

d) Face indexing of crystals from 1-octanol:
The morphology of DHC-II crystals obtained form 1-octanol as solvent differed significantly from the morphology of DHC-II crystals obtained from ethylacetate solution. Face indexing of crystals from 1-octanol are shown in figure S11 (a) (b). Whilst the morphology does not match exactly with the computationally predicted morphology, it agrees in the dominance of the large (001) face (Figure S48). The morphologies of the DHC-II crystals grown from ethylacetate have far higher aspect ratio and feature ledges.

However, due to slow evaporating nature of 1-octanol, ethyl acetate was chosen as the preferred solvent system to obtain DHC-II crystals.

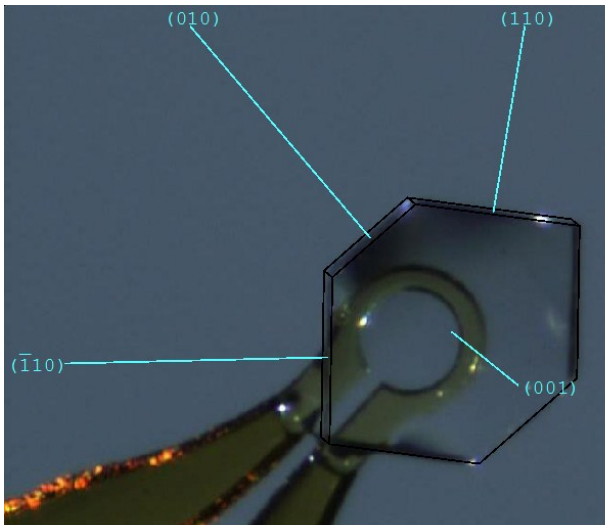

(a)

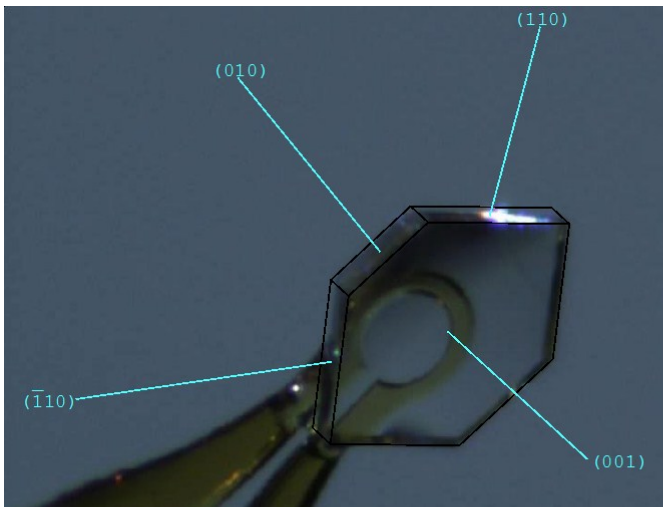

(b)

Figure S11 (a) and (b): face indexing of DHC-II crystals obtained form 1-octanol.

4. Results from sublimation experiments

a) Optical microscope images of material obtained from sublimation experiments. Microscope images of material from vapour deposition of CBZ on DHC-II.

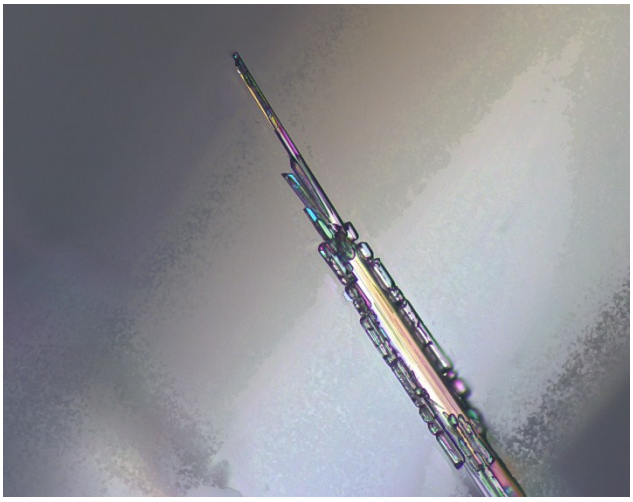

Figure S12: CBZ-V on DHC-II

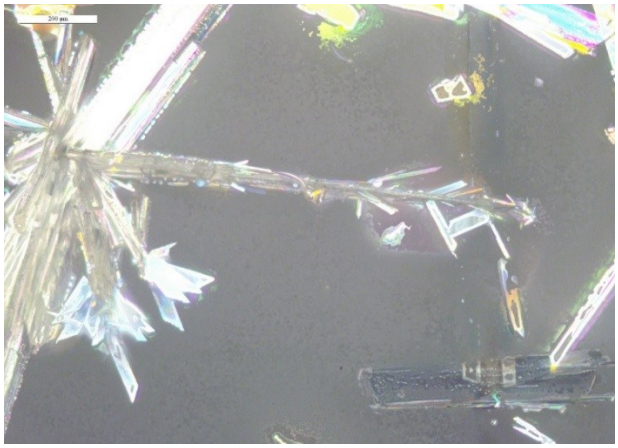

Figure S13: CBZ on DHC-II crystals

Figure S14: CBZ crystals growing on DHC-II surface.

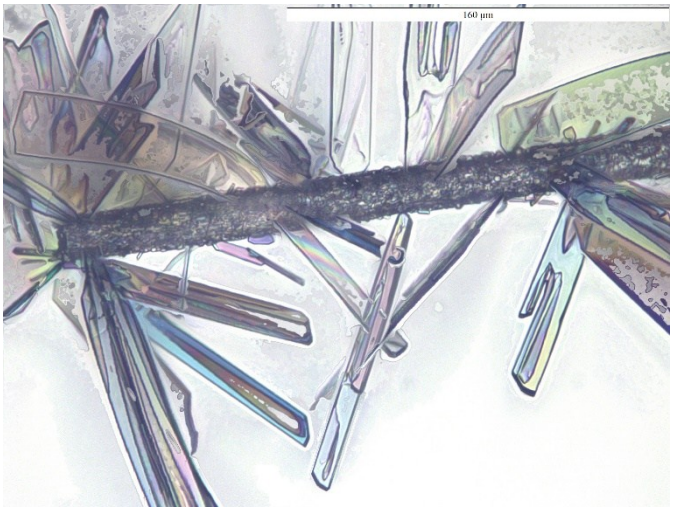

Figure S15: CBZ on DHC-II.

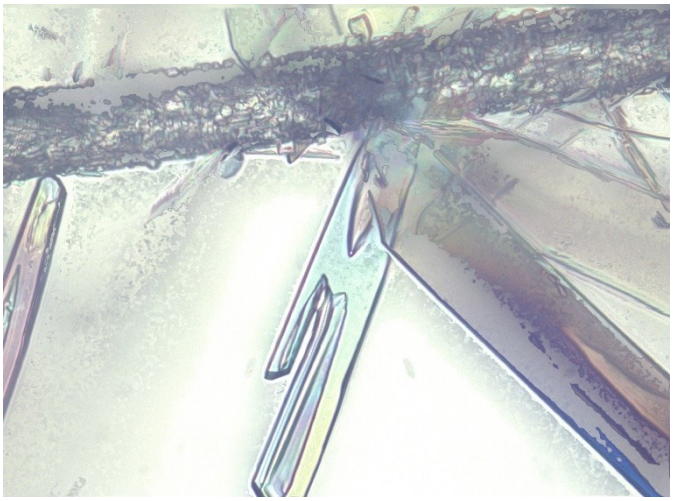

Figure S16: CBZ crystals growing on DHC-II surface.

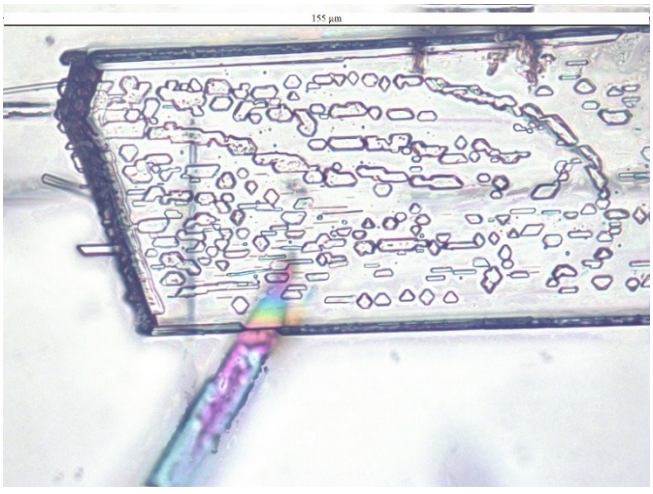

Figure S17: CBZ crystals growing on DHC-II surface.

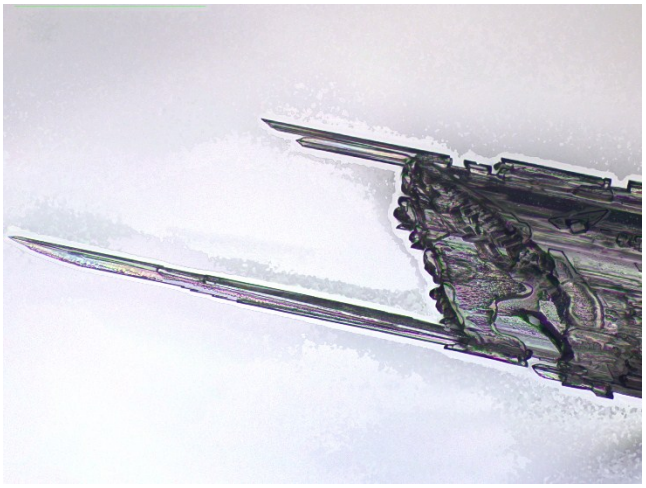

Figure S18: CBZ crystals growing on DHC-II surface.

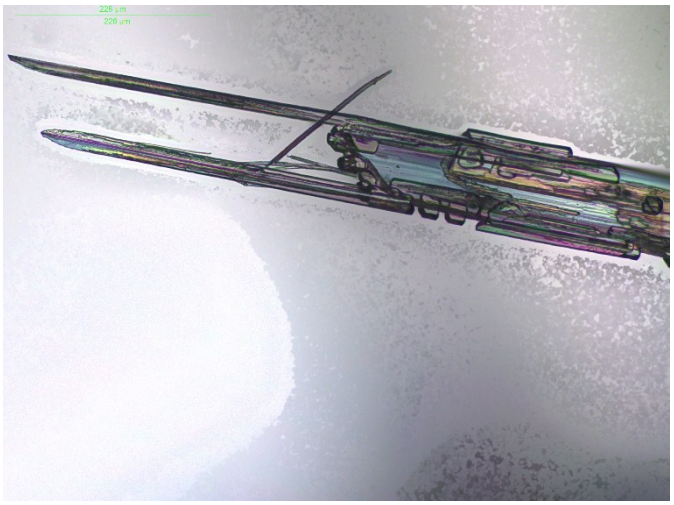

Figure S19: CBZ crystals growing on DHC-II surface.

.

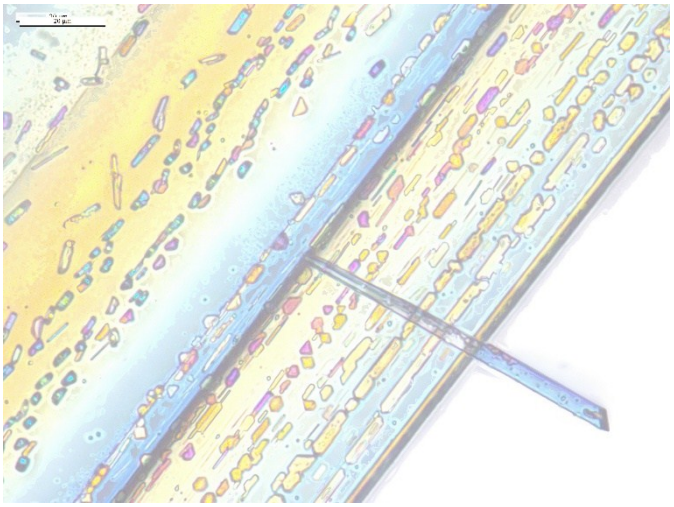

Figure S20: CBZ crystals growing on DHC-II surface.

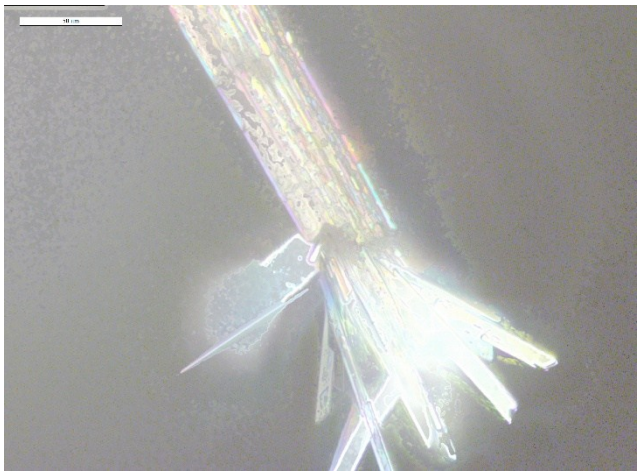

Figure S21: CBZ crystals growing on DHC-II surface.

Fig S22: CBZ on DHC-II

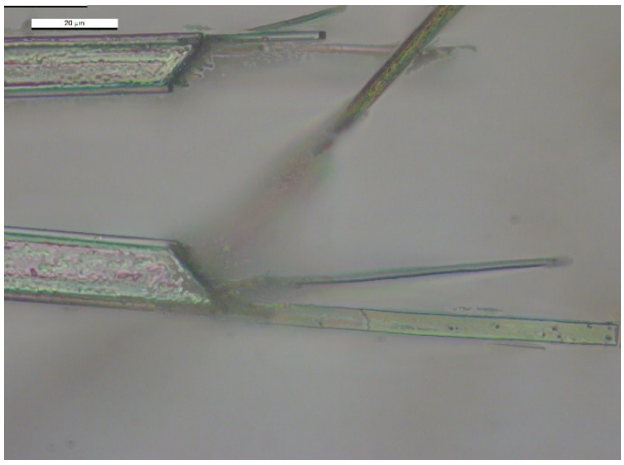

Fig S23: CBZ on DHC-II

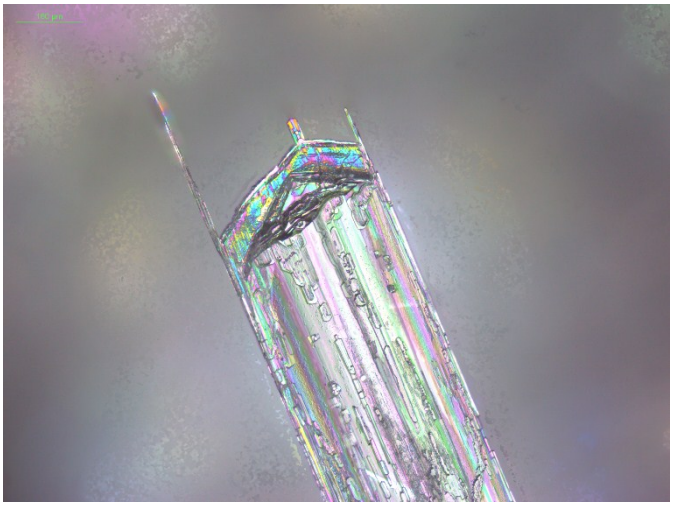

Fig S24: CBZ on DHC-II

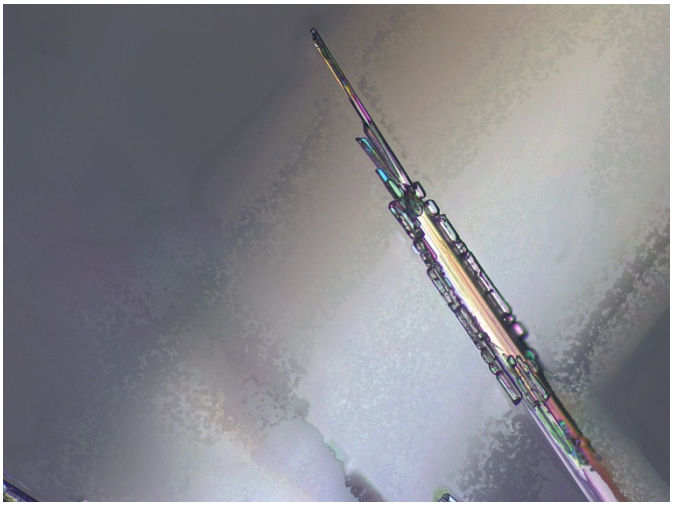

Fig S25: CBZ on DHC-II

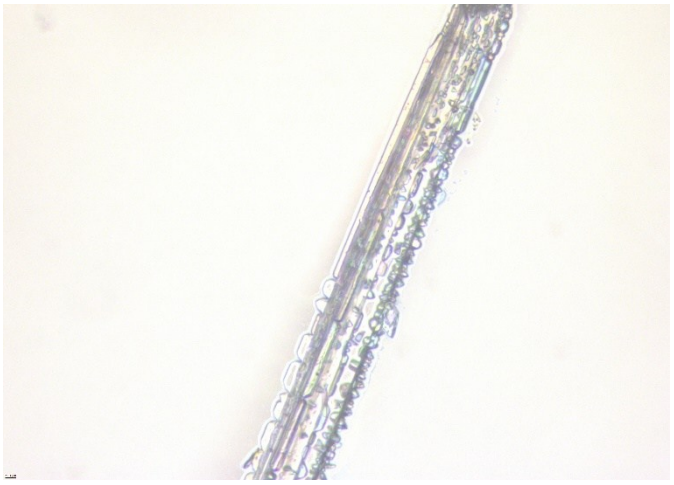

Fig S26: CBZ on DHC-II

Powder X-ray diffraction analysis was performed on DHC-II crystals from the sublimation experiments. Whilst there is the expected preferred orientation there are no peaks belonging to CBZ Form-I suggesting that the microcrystals on the DHC-II could be CBZ-V.

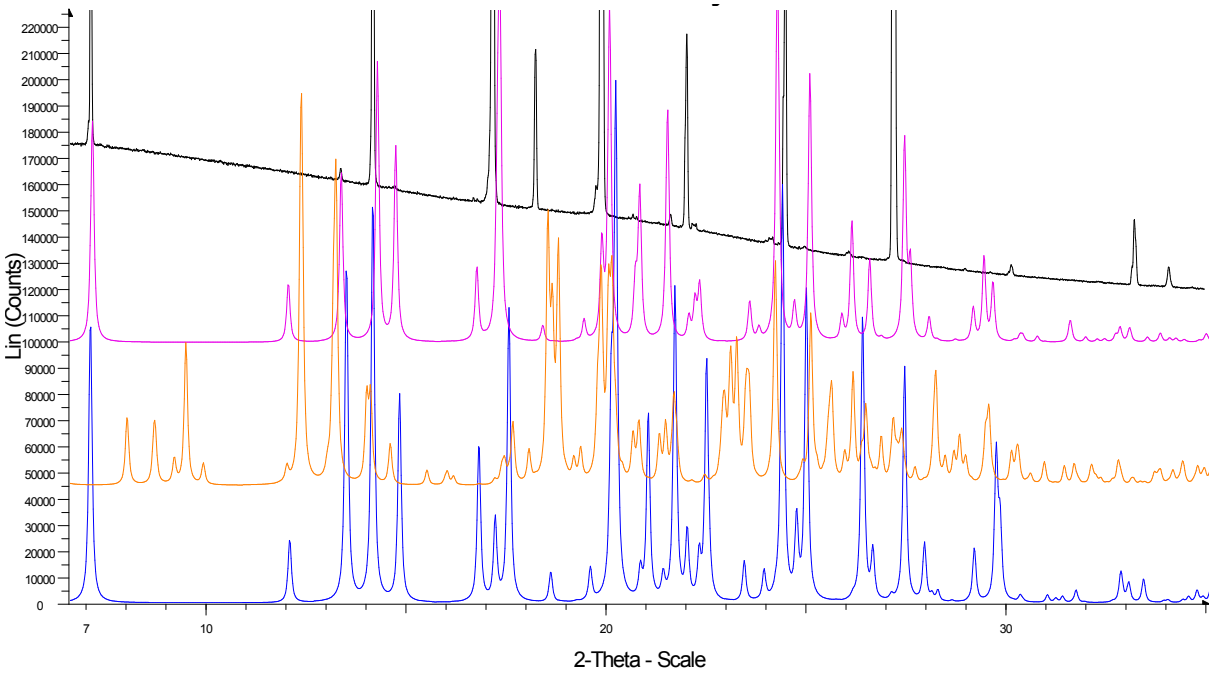

Figure S27: PXRD comparison plot of DHC-II single crystals form sublimation (black) with single crystal simulated powder pattern of CBZ-V (pink), CBZ-I (orange) and DHC-II (blue).

b) Microscope images of material from vapour deposition of CYH on DHC-II single crystals

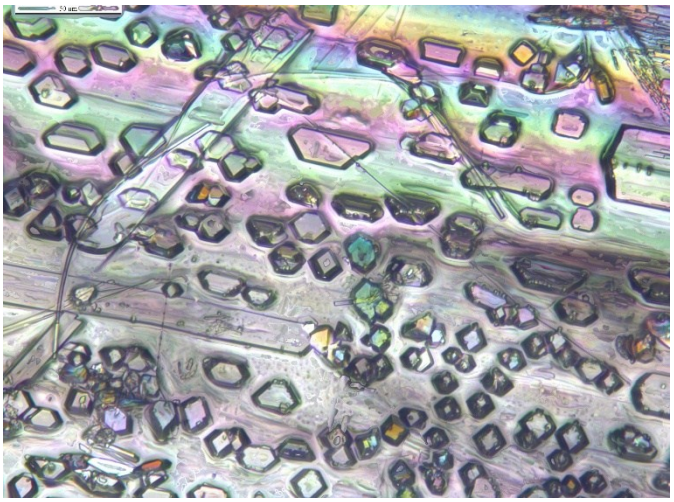

Fig S28: CYH on DHC-II

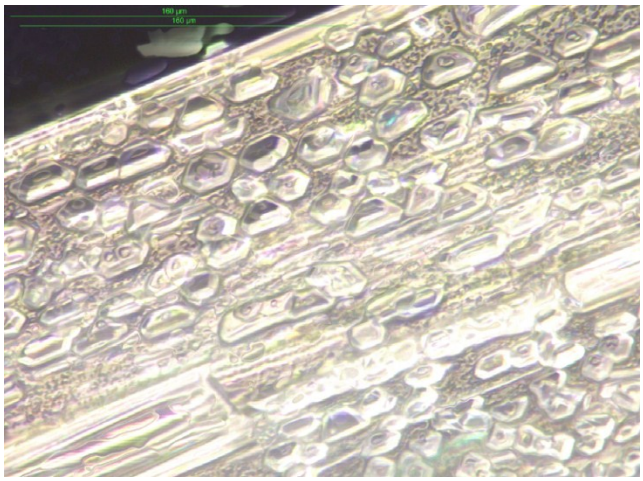

Figure S29: CYH on DHC-II

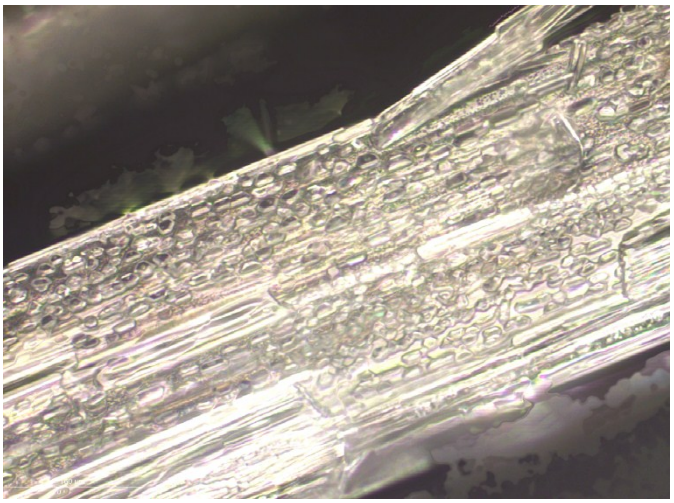

Figure S30: CYH on DHC-II

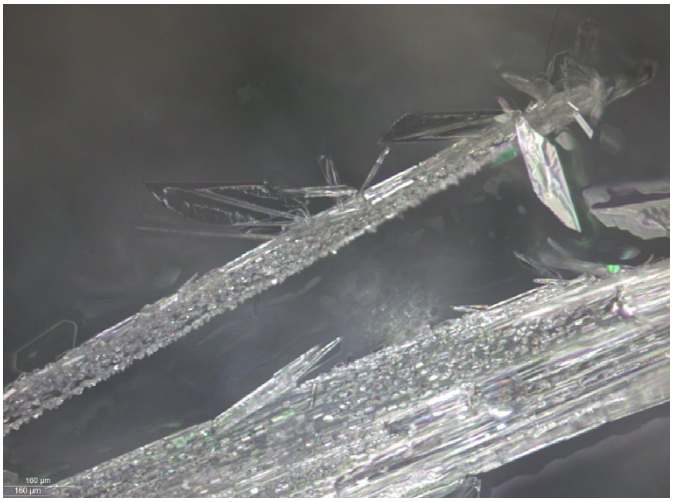

Figure S31: CYH on DHC

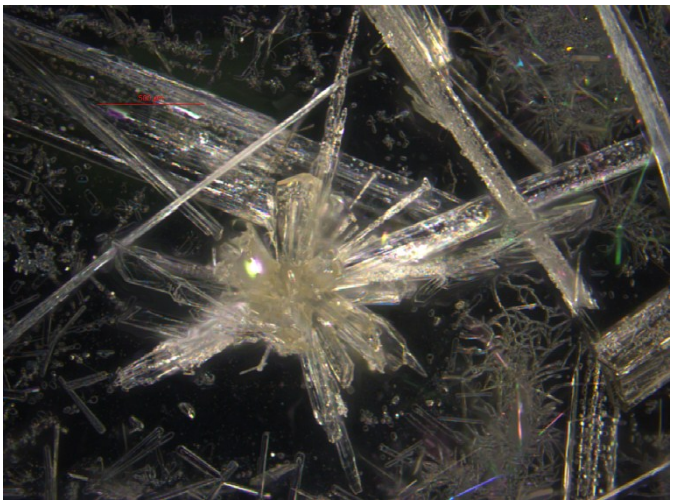

Fig S32: CYH on DHC-II

c) Microscope images of material from vapour deposition of DHC on DHC-II single crystals

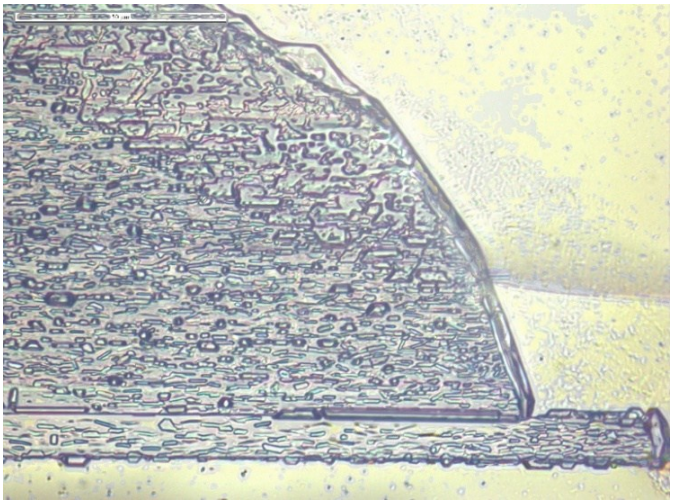

Fig S33: DHC on DHC-II

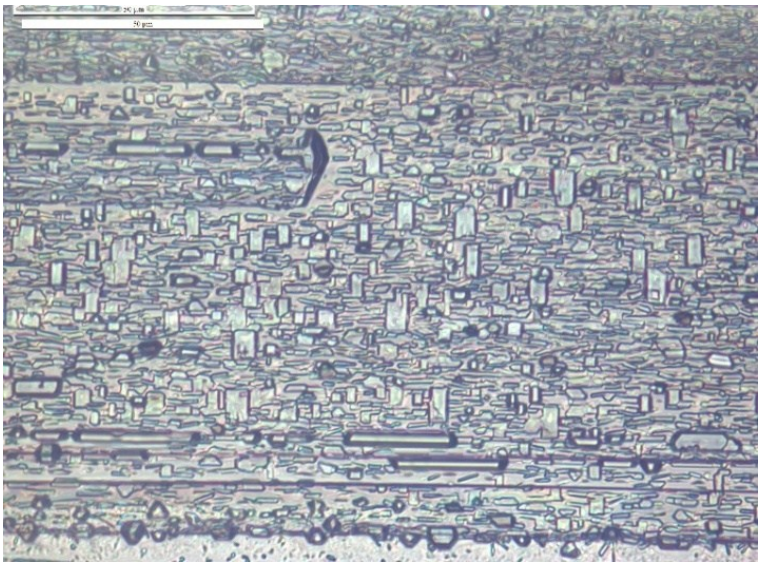

Fig S34: DHC on DHC-II

d) Raman analysis of DHC-II, CBZ-V and CYH-III.

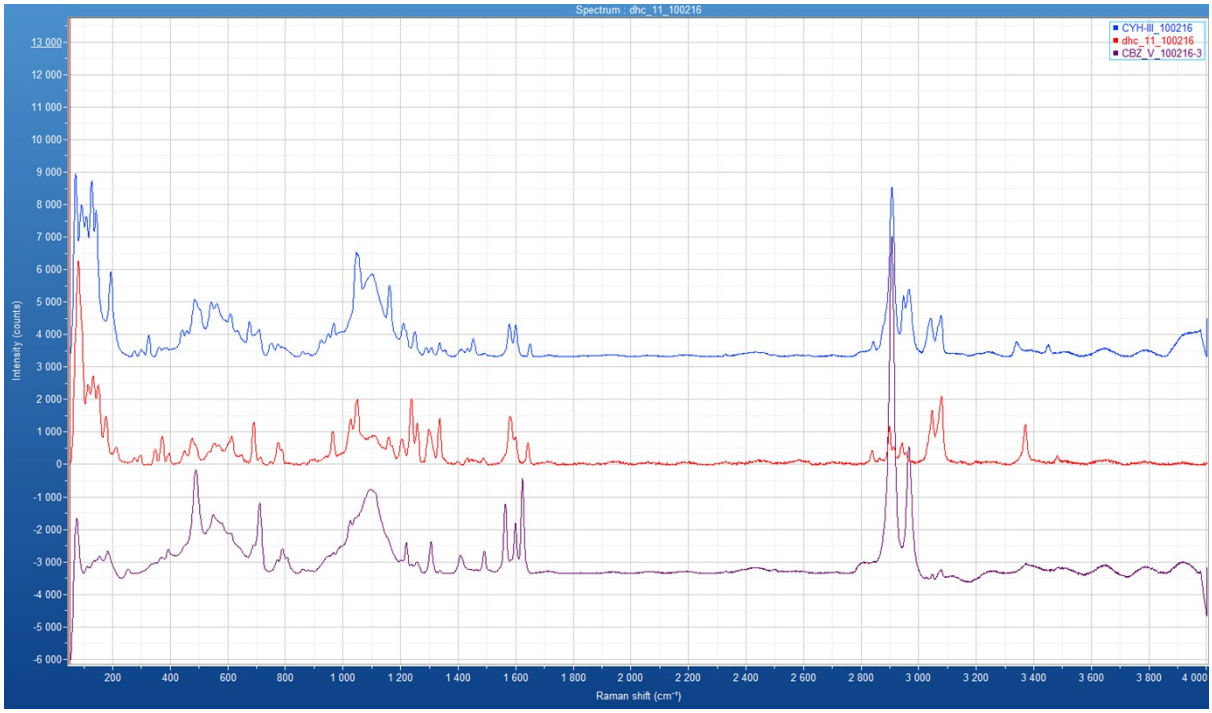

Fig S35: Comparison plot of Raman analysis of DHC-II, CBZ-V and CYH-III.

5. Crystallographic data of CYH-III.

Table S1: Crystallographic data of CYH-III.

	Cyheptamide form-III
chemical formula	$C_{16}H_{15}N_1O_1$
formula weight	237.3
crystal system	orthorhombic
a (Å)	9.0171 (5)
b (Å)	11.0071 (6)
c (Å)	23.9483 (13)
α, β, γ/(°)	90.0
Space group	Pbca
V/(Å)^3	2376.9 (2)
Z	8
$N_{reflection}/N_{parameter}$	1991/169
ρ_{calc}/ g cm^{-3}	1.326
radiation type	Cu Kα (λ = 1.5418 Å)
T/K	123
θ range/°	6 – 75
range of h	-10 to 11
range of k	-13 to 13
range of l	-29 to 29
R merge	0.06
R_1 (%)	4.4
WR_2 (%)	4.6
goodness-of-fit	0.891

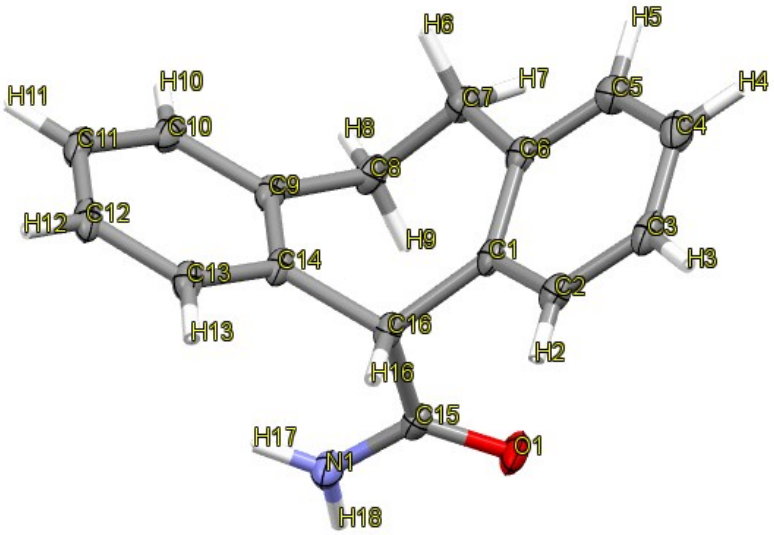

Figure S36: ORTEP of CYH-III.

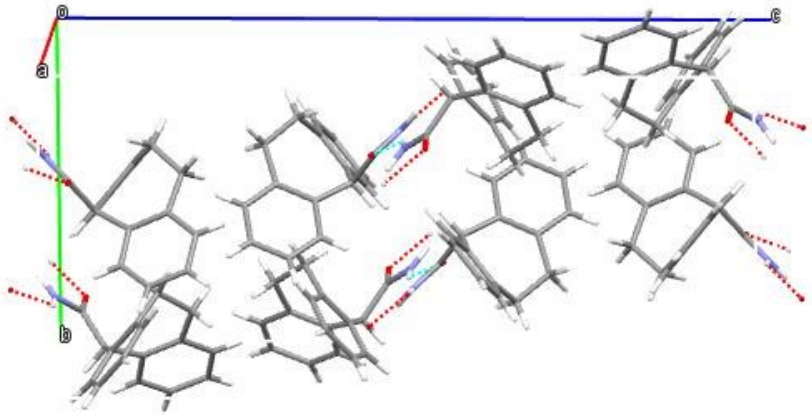

Figure S37: Crystal packing arrangement of CYH-III viewed approximately down the hydrogen bonding chains.

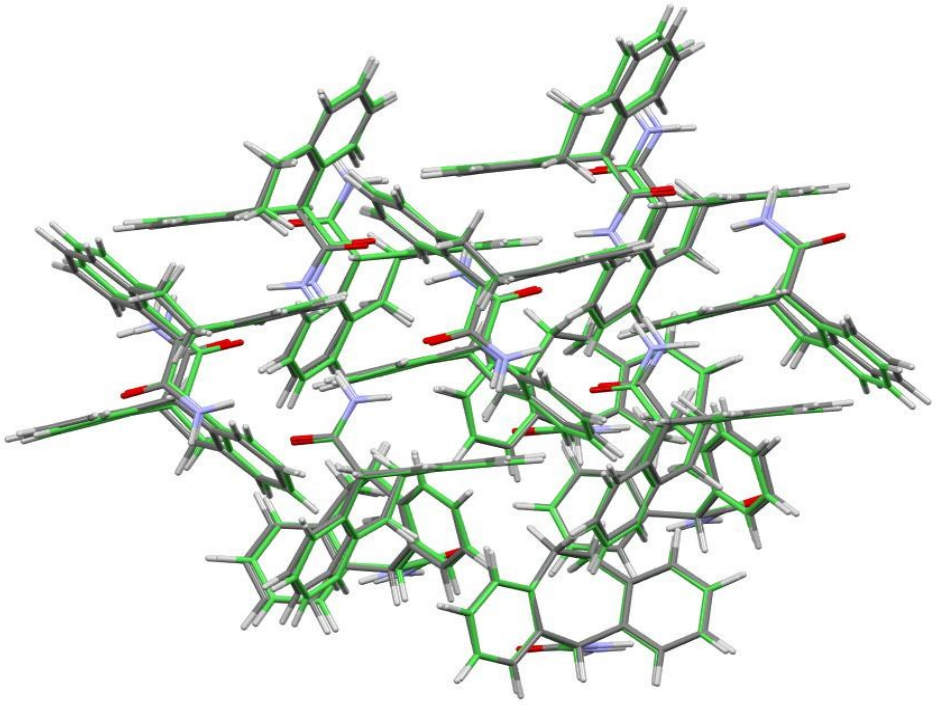

Figure S38: Overlay of predicted CSP#16 (green) and experimental (grey) crystal structures (RMS_{15}=0.196 Å).

II. Crystal energy landscape of cyheptamide.

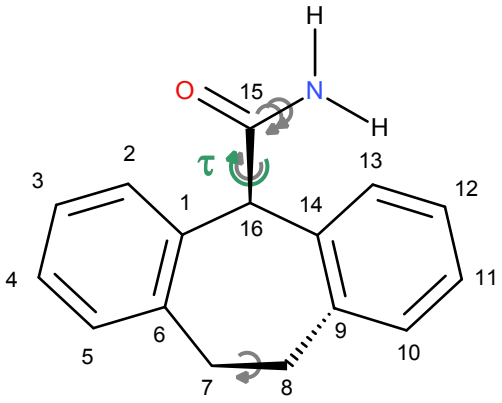

Figure S39: Numbering convention for cyheptamide used in the computational work and for form III.cif file. Green arrows denoted the only torsion angle (τ: C1-C16-C15-N) varied in the CrystalPredictor search with grey arrows depicting the torsion angles refined by CrystalOptimizer.

Unlike CBZ, DHC and CYH have inequivalent syn and anti conformers with respect to the amide group, from the C7-C8 bond orientation. CYH form 1 (TEVSOD, P21/c, Z'=1, isostructural to DHC form I) has the molecules in the anti conformation forming hydrogen-bonded catemers and form II (TEVSOD01, P-1, Z'=4, isostructural to CBZ form I) forms hydrogen-bonded dimers involving three anti and one syn conformation. The energy difference between the two conformers in isolation is very small, ranging from -0.48 to 1.63 kJ/mol for various computational models, with the density functional based methods having the syn conformer more stable. This introduces some uncertainty into the relative lattice energies. The torsional potential energy profile for the syn to anti conformational change used in the CrystalPredictor search is shown in Figure S40.

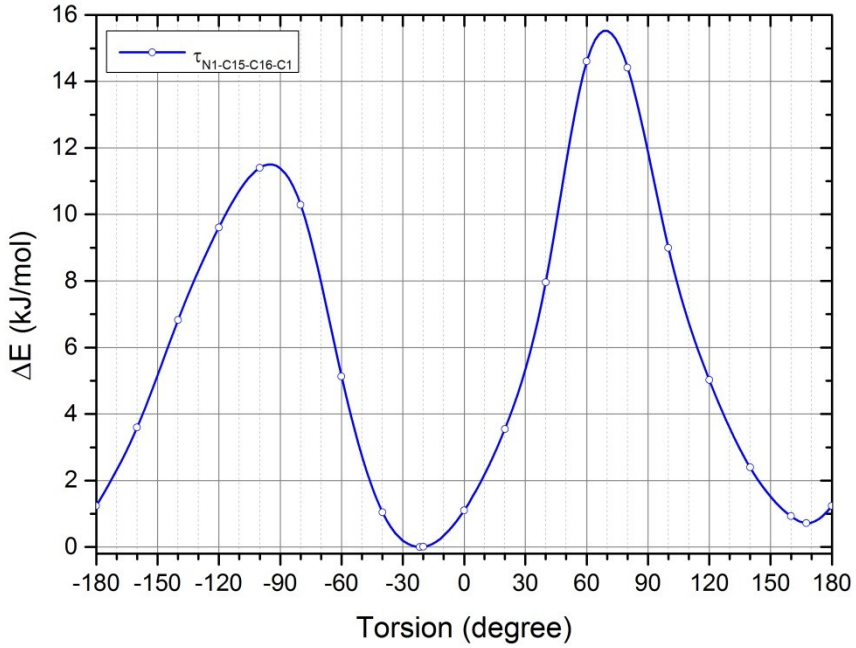

Figure S40: Gas-phase cyheptamide potential energy curve along the C1-C16-C15-N torsion angle scanned at PBE0/6-31G(d,p) level using GAUSSIAN. All other molecular degrees of freedom were allowed to relax. The minimum in the syn conformation is –21.7° and the anti is 167.4°.

The CSP structure generation was carried out with CrystalPredictor ver. 2.0.1, allowing the C1-C16-C15-N torsion to vary over the complete range shown in Figure S40. A million initial structures of cyheptamide with Z'=1 in the 60 most common space groups were generated. These were minimised with the FIT potential and atomic charges derived by fitting to the molecular electrostatic potential around the nearest grid point calculated at PBE0/6-31G(d,p) level. After the minimisations, ANALYSE (ver. 2.0.1) was used to cluster the structures, giving 13205 unique crystal structures within 30 kJ/mol of the CrystalPredictor global minimum, shown in Figure S41. The structures are labelled by their energy ranking at this stage.

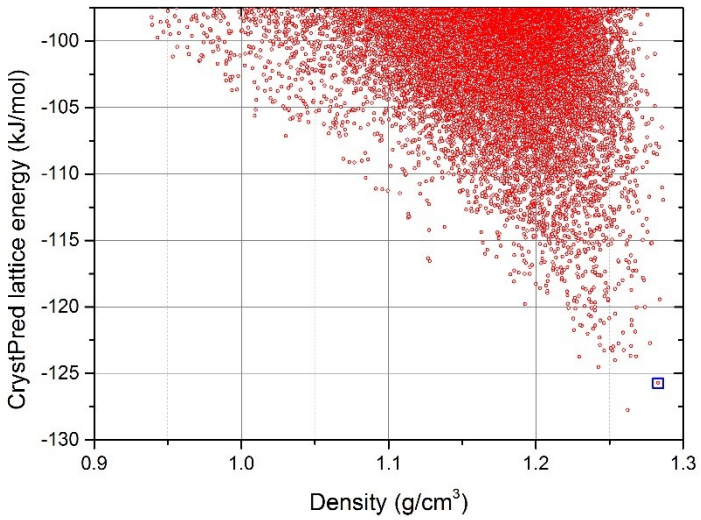

Figure S41: CrystalPredictor lattice energy landscape after one million structures were generated. Only unique structures within 30 kJ/mol of the global minimum are shown. The blue square indicates the structure corresponds to experimentally observed CYH form I.

All the 2260 unique structures up to 21.9 kJ/mol above the global minimum in Figure S41 were refined using CrystalOptimizer ver. 2.2, allowing the C1-C16-C15-N, O-C15-C16-C1, C6-C7-C8-C9, H11-N-C15-C16 and H12-N-C15-C16 torsions to vary. Multipole derivatives for the two H-N-C15-C16 torsions were used to improve the description of distributed multipoles of the electron lone pair on the nitrogen atom, which changes with the pyramidalization of -NH2 group, generating Figure S42. The 141 unique structures within 15 kJ/mol are shown in the summary of the CSP search, Figure S43. The global minimum of the search corresponds to the experimentally observed form I of CYH, with a $Rmsd_{15}$ of 0.177 Å. The CSP study with Z'=1 cannot find the Z'=4 experimental form II of CYH, so it was optimized with the same model for comparison.

Figure S42 analyses the CSP generated structures by the N-C15-C16-C1 torsion, showing that all the lower energy structures are around the syn or anti conformations, with other conformations being high in lattice energy. The packing coefficients of cyheptamide were calculated with CCDC software packingcoefficients using 0.1 Å grid spacing, and which shows (Figure S43) that cyheptamide is able to pack quite densely, with the packing coefficients up to ~ 73%, i.e. close to the hard-sphere packing.

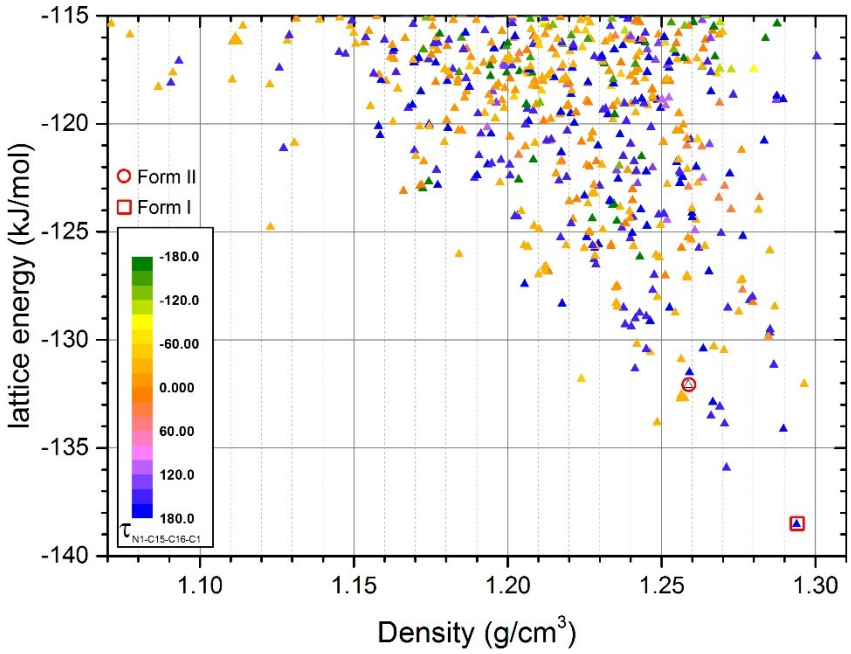

Figure S42: CrystalOptimizer lattice energy landscape of cyheptamide. Each structure was colour-coded with respect to its N-C15-C16-C1 torsion angle. The corresponding minima for the originally known forms I and II of cyheptamide are shown.

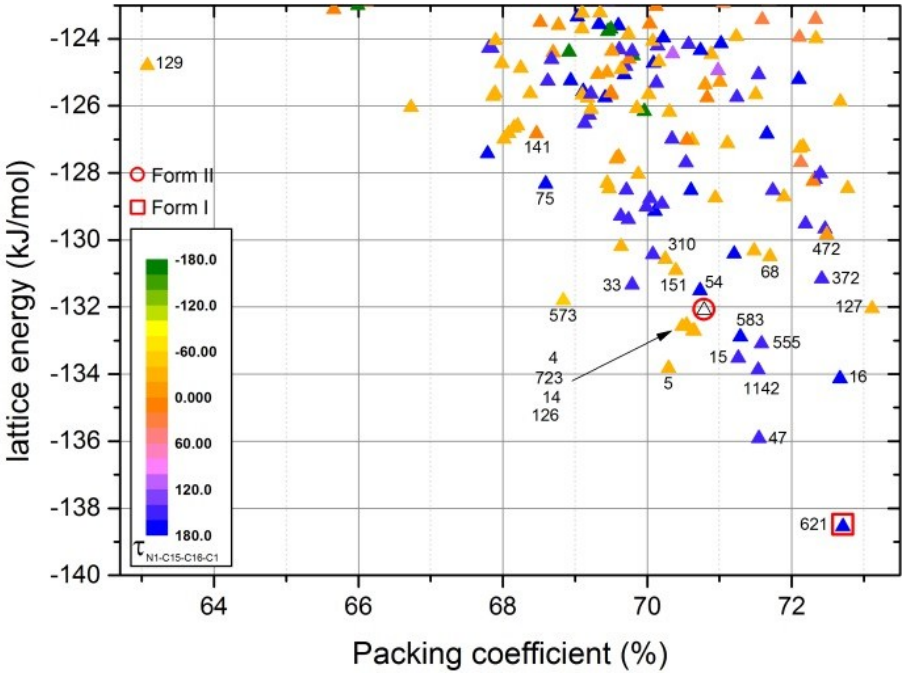

Figure S43: Summary of the CSP study of CYH, with the energies from CrystalOptimizer (FIT+ DMA(PBE0/631G(d,p) +ΔEintra(PBE0/631G(d,p)). Each symbol represents a stable crystal structure, coloured by the torsion angle. The minima corresponding to the previously known forms are outlined in red. The numbers labelling the structures correspond to their energy ranking after CrystalPredictor and their cell dimensions are given in Table S2.

The sensitivity of the relative energies to the assumed model for the intermolecular forces was tested by first considering the polarisation that occurs in the crystal by recalculating the intramolecular energy and distributed multipoles in a polarisable environment with ε=3 in

GAUSSIAN. As a further test, the Helmholtz free energy (FE) of each crystal structure at 298 K was derived from the harmonic rigid-body elastic constants and k=0 phonons.

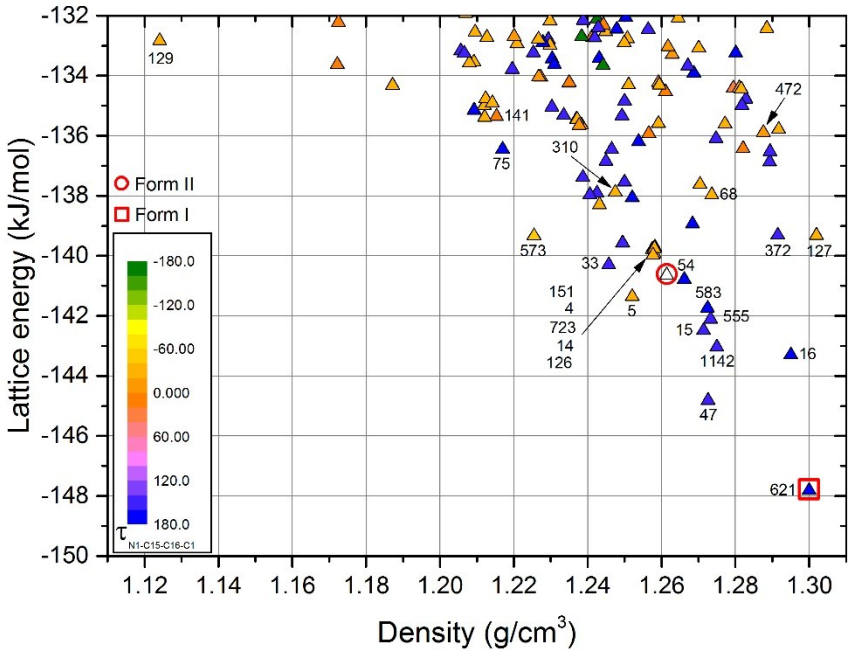

Figure S44: PCM lattice energy landscape of cyheptamide calculated at FIT/PBE0/6-31G(d,p) level. PCM(ε=3) was chosen to simulate the usual environment in organic crystals.

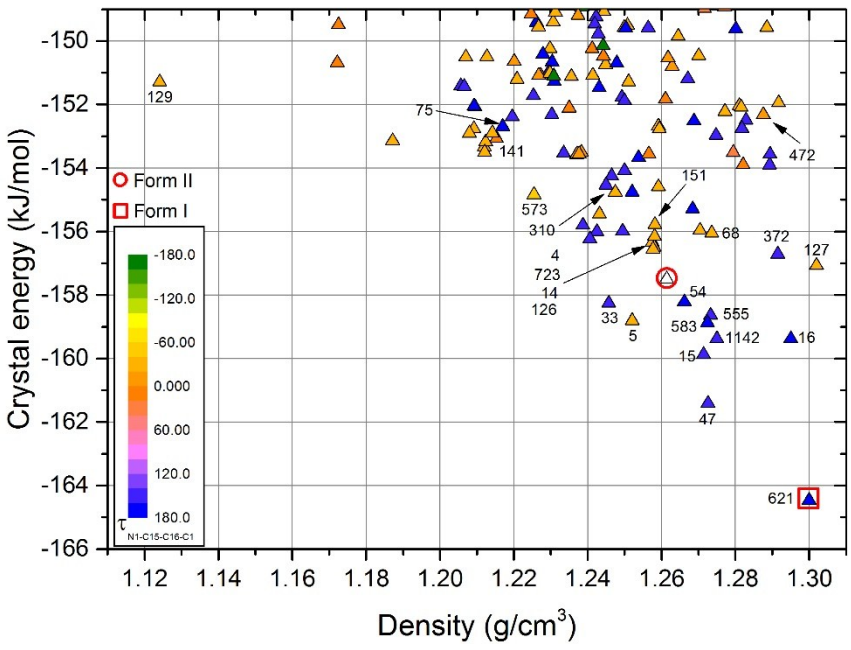

Figure S45: Crystal energy landscape of CYH CSP structures at 298K.This plot corresponds to Figure 3 in the m/s, but is based on conformation and has all the structures in Table 1 labelled.

Comparison of Figures S43-S45 shows that the same set of structures, given in Table 1, are competitive with the known polymorph CYH II and so can be considered as thermodynamically plausible polymorphs. All these crystal structures were compared with the known polymorphs of DHC and CBZ using the Crystal Packing Similarity function in Mercury[1] and confirmed by XPAC

analysis[2]. A candidate structure (CYH#16) was found in Pbca space group with cell parameters very similar to those of CBZ form V and DHC form II (Table 1 of m/s). Hence the low energy and high density of CYH#16 showed that it was worth testing the generality of the templating method that had produced CBZ V to find CYH III.

Table S2: Crystal structures for CYH generated by CSP. Structures corresponding to experimental forms are shaded in green. The full structures in .res format are available from the UCL authors on request.

Structure			a (Å)	b (Å)	c (Å)	α (°)	β (°)	γ (°)	Density (g/cm3)	ΔElatt (kJ/mol)
Catemer-based										
CYH#621	P21/n	anti	5.5766	9.3851	23.3649	90	84.95	90	1.2939	0.00
CYH#16	Pbca	anti	9.2878	11.0190	23.8845	90	90	90	1.2896	4.41
CYH#1142	P21/c	anti	12.7116	5.6303	18.2942	90	71.35	90	1.2705	4.66
CYH#15	P21/n	anti	9.5227	5.4501	23.9883	90	90.60	90	1.2661	5.02
CYH#555	P21/a	anti	18.3291	5.5848	12.7924	90	71.53	90	1.2690	5.45
CYH#583	P212121	anti	9.3083	23.8902	5.5953	90	90	90	1.2667	5.65
CYH#127	P21/c	syn	5.5226	23.3182	9.4463	90	88.06	90	1.2964	6.50
CYH#54	Pca21	anti	23.5561	5.5689	9.5427	90	90	90	1.2591	7.04
CYH#372	P21/a	anti	9.3166	23.7296	5.5439	90	88.45	90	1.2865	7.38
CYH#68	P21/n	syn	22.4159	9.9783	5.5594	90	86.25	90	1.2703	8.05
Dimer-based										
CYH#47	P-1	anti	12.6530	9.2627	5.6335	87.58	85.90	70.32	1.2711	2.62
CYH#5	P21/n	syn	12.8507	5.5786	18.2644	90	74.60	90	1.2486	4.72
CYH#723	P-1	syn	12.7847	5.5725	9.4619	88.18	111.36	89.65	1.2561	5.82
CYH#4	P-1	syn	9.7387	5.5472	12.3925	91.76	69.60	92.77	1.2576	5.83
CYH#14	P-1	syn	12.7885	5.5722	9.4526	88.15	68.73	90.29	1.2564	5.96
CYH#126	P-1	syn	12.4084	9.7317	5.5431	87.32	88.21	69.74	1.2565	6.01
CYH#573	R-3	syn	34.4215	34.4215	5.6479	90	90	120	1.2239	6.74
CYH#33	P21/n	anti	13.1516	5.4803	18.3952	90	73.26	90	1.2414	7.21
CYH#151	P21/n	syn	13.7980	7.9572	11.7892	90	75.74	90	1.2564	7.63
CYH#310	P21/n	syn	12.5269	5.5210	19.2611	90	71.69	90	1.2463	7.97
CYH#75	R-3	anti	34.5051	34.5051	5.6492	90	90	120	1.2177	10.21
Form II	P-1	anti & syn	5.7096	19.9764	22.2037	84.10	88.37	83.89	1.2587	6.45
Others										
CYH#472	P212121	Syn	19.9121	7.9841	7.7165	90	90	90	1.2848	8.70

Further energy calculations on the CYH polymorphs

To further check the sensitivity of the lattice energy to the assumptions made in the modelling, periodic density functional calculations were performed using CASTEP ver. 7.02 on UK National High Performance Computing Facility (ARCHER). A cutoff of 700 eV and k-point spacing of 0.04 $Å^{-1}$ were used in optimisations of the crystal structures using the PBE functional with TS dispersion correction. Different dispersion correction schemes were compared by carryiong out a single point PBE+G06 calculation on each PBE+TS optimised crystal structure (denoted as PBE+TS/PBE+G06) in Table 2.

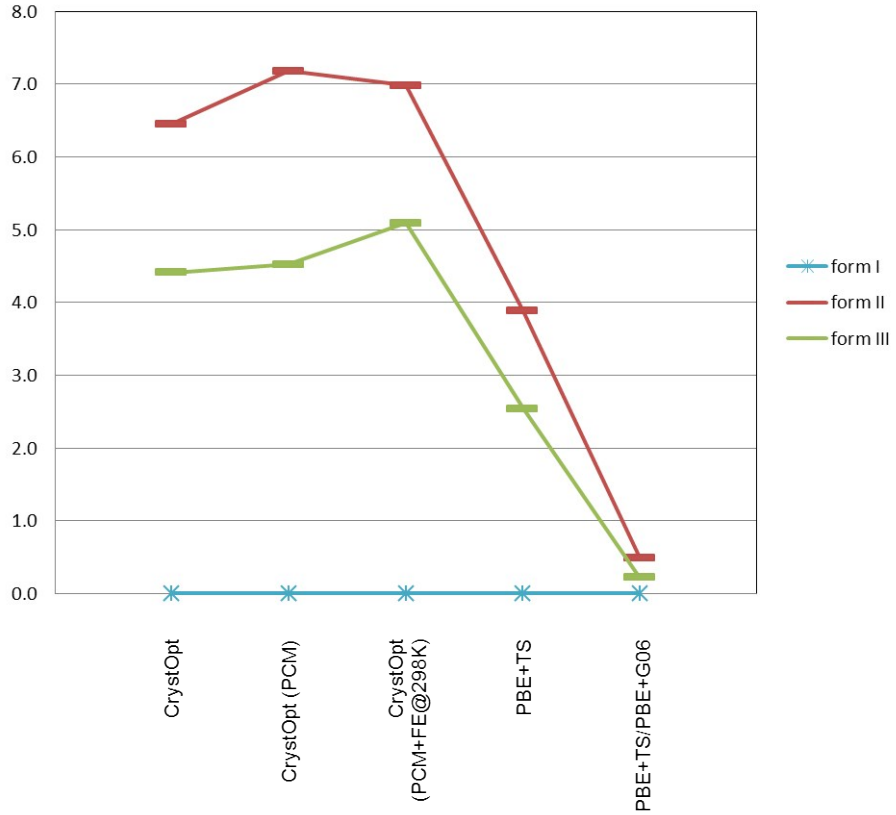

Figure S46: Relative energetics of the three forms of CYH calculated with the three methods used for the crystal energy landscapes CrystOpt(Figure S43), with PCM (Figure S44) and free energy estimate (Figure S45) and with periodic electronic structure calculations.

Table S3: Results of DFT+D optimisation for CYH polymorphs.

	a (Å)	b (Å)	c (Å)	α (°)	β (°)	γ (°)	ΔElatt (kJ/mol)	
							PBE+TS	PBE+G06 /PBE+TS
Form I exp.	5.6035	9.1716	23.5790	90	96.75	90		
Form I calc.	5.5220	9.1430	23.3399	90	97.02	90	0.0	0.0
Form II exp.	5.6491	19.5639	22.0741	84.22	88.41	83.60		
Form II calc.	5.5376	19.5697	21.9337	84.21	88.82	83.76	3.65	0.49
Form III exp.	9.0171	11.0071	23.9483	90	90	90		
Form III calc.	9.0392	10.8748	23.6029	90	90	90	2.35	0.22

Morphological analysis:

Experimental face indexing of templating crystals grown from ethyl acetate, contrasted with those from 1-octanol, indicates that there is a significant solvent effect on the morphology. Comparison of these morphologies with those generated by the BDFH model (Figure S47) and by the attachment energy model, suggest that the crystal growth in 1-octanol is less affected by solvent than growth from ethyl acetate.

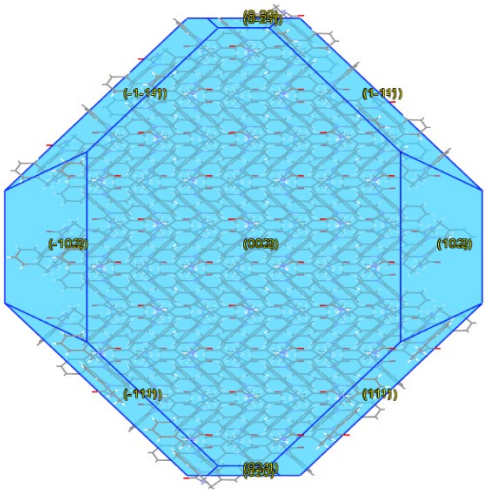

Figure S47: BDFH morphology of DHC-II model from Mercury.

The morphologies of the Z'=1 polymorphs of CYH were calculated using the attachment energy model (Figure S48) using the same repulsion-dispersion potential and potential-derived atomic charges as used in CrystalPredictor search. The relative growth volumes[3] of 1.37 suggest that form III could grow more readily than form I. This however, is within the limitations of the attachment energy model for morphologies, which is applicable only for sublimation grown crystals below the roughening temperature.

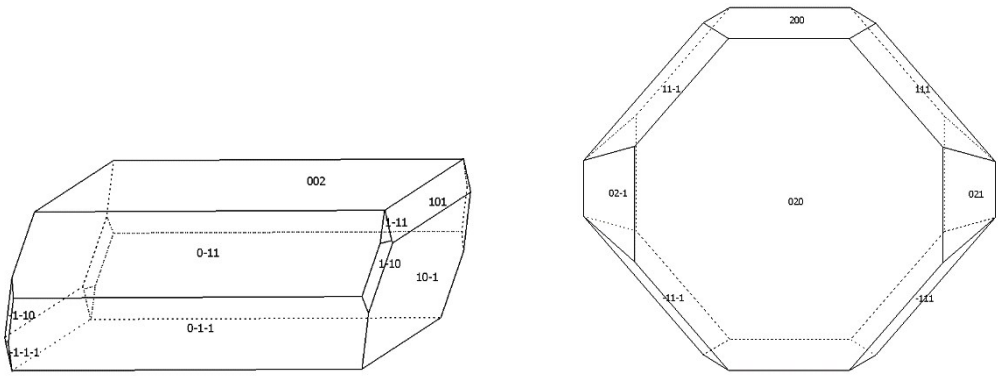

CSP#621 ~ CYH I **CSP#16 ~ CYH III**

Figure S48: Attachment energy morphology predictions.

III. References

1. Macrae, C. F.; Edgington, P. R.; McCabe, P.; Pidcock, E.; Shields, G. P.; Taylor, R.; Towler, M.; van de Streek, J., Mercury: visualization and analysis of crystal structures. Journal of Applied Crystallography 2006, 39, 453-457.

2. Gelbrich, T.; Hursthouse, M. B., A versatile procedure for the identification, description and quantification of structural similarity in molecular crystals. CrystEngComm 2005, 7, 324-336.

3. Coombes, D. S.; Catlow, C. R. A.; Gale, J. D.; Rohl, A. L.; Price, S. L., Calculation of attachment energies and relative volume growth rates as an aid to polymorph prediction. Crystal Growth & Design 2005, 5 (3), 879-885.